A two-dimensional finite volume unstructured mesh method for transient simulation of time- and scale-dependent transport in heterogeneous aquifer systems

F. Liu, I. Turner, V. Anh and N. Su

School of Mathematical Sciences
Queensland University of Technology, Gardens Point Campus
GPO Box 2434, Brisbane, Qld. 4001, Australia

ABSTRACT

In this paper, solute transport in heterogeneous aquifers using a modified Fokker-Planck equation (MFPE) is investigated. This newly developed mathematical model is characterised with a time-, scale- and density-dependent dispersivity. A two-dimensional finite volume unstructured mesh method (FVUMM) is developed for analysing the model. The FVUMM transforms the coupled non-linear partial differential equations into a system of differential/algebraic equations, and is solved by backward differentiation formulas of order one through five in order to advance the solution in time. Henry's classic benchmark problem is used to show that the MFPE captures significant features of transport phenomena in heterogeneous porous media including enhanced transport of salt in the upper layer due to its parameters that represent the dependence of transport processes on scale and time. The time and scale effects are investigated, and numerical results are compared with published results on the same problems.

1. Introduction

Saltwater intrusion occurs in coastal regions in many parts of the world. Because of the environmental and economical importance, investigation into the pathways and patterns of seawater intrusion is crucial in coastal regions where seawater intrusion is a concern. There are different objectives as far as the studies of seawater intrusion are concerned; the need for predicting the location and movement of the seawater interface is one of the major issues that needs to be addressed in order to protect freshwater aquifers.

As early as 1964, Henry developed the first solution for the steady-state salt distribution in a confined coastal aquifer. In many cases, however, the production of a steady-state solution from transient simulations is not feasible due to its high computing costs. Segol et al [1975] developed the first transient solution based on a velocity-dependent dispersion coefficient using the Galerkin finite element method to solve a set of non-linear partial differential equations that describe the movement of a saltwater front in a coastal confined aquifer. Frind [1982a, 1982b], Voss [1984], and Cheng et al [1998] also developed numerical methods for simulating seawater intrusion. Density-dependence of salt transport in aquifers is not the main concern.. For solute transport processes in subsurface flow in porous media, extensive field tracer studies in the past decades have also generated concerns about the scale effect [Lallemand-Barres and Peaudeserf, 1978; Neuman, 1990; Gelhar et al, 1992] due to the heterogeneity of aquifers. While a great deal of effort has been expended to investigate the scale effect in the dispersion coefficient, less attention has been paid to the equally important issue of the time effect [Dieulin, et al, 1981; Hentschel and Procaccia, 1984] on the dispersion coefficient. The development is made possible by incorporating a modified fractal model developed by Wheatcraft and Tyler [1988] to take into account spatial variability and a temporal component to embrace the effect of time or age on diffusion [Muralidhar and

Ramkrishna, 1993, p. 88–89]. In this paper, we combine the time-, scale-, and density-dependence of transport in heterogeneous aquifer systems to investigate various hydrological and mathematical characteristics of the model performance. The problem is formulated in terms of two tightly coupled, non-linear partial differential equations. The first equation describes the flow of a variable-density fluid and the second the transport of dissolved salts with time- and scale-dependent dispersivity. Because of the inherently complex boundary conditions and physical geometries in any practical transient simulation of time- and scale-dependent transport in heterogeneous porous media, it is not possible to obtain analytical solutions, hence appropriate numerical methods have to be used. This paper presents a finite volume unstructured mesh method for the transient problem. The coupled partial differential equations are transformed by FVUMM into a system of differential-algebraic equations. This system then is solved by using the backward differentiation formulas of order one through five [Pelzold, 1982]. Three examples are given, namely, saltwater intrusion into a confined aquifer, saltwater intrusion in a phreatic aquifer, and leachate transport in an unconfined aquifer. Simulated results are compared to published solutions, and the time and scale effects are investigated using Henry's saltwater intrusion problem with explanations provided about realistic phenomena captured by MFPE.

2. Statement of the Problem

Time-, scale- and density-dependent transport in heterogeneous aquifers is analysed in the context of saltwater intrusion. The time- and scale-dependent transport phenomena are captured via the dispersion tensor in the transport equation, and density-dependence of transport is implemented in Darcy's law. The dispersion is governed by a coupled non-linear system of two partial differential equations. The first differential equation is the flow equation that describes the head distribution in the aquifer of interest.

The pressure head variable commonly used in the flow equation has been replaced by an equivalent freshwater head that generally results in the elimination of static quantities and improves numerical efficiency [Frind, 1982b].

The flow equation may be written as [Frind, 1982a, 1982b; Huyakorn et al., 1987]

$$S_s \frac{\partial h}{\partial t} = \nabla \cdot \left[\mathbf{K} \left(\nabla h + \gamma C \nabla z \right) \right] \tag{1}$$

where

h is the reference hydraulic head referred to as the freshwater head;

$\mathbf{K}$ is the hydraulic conductivity tensor;

γ is the density coupling coefficient;

C is the solute concentration;

S_s is the specific storage;

t is time; and

z is elevation.

The reference head and the density-coupling coefficient in (1) are defined as

$$h = \frac{p}{\rho_0 g} + z \tag{2}$$

and

$$\gamma = \frac{\varepsilon}{C_{\max}} \tag{3}$$

where

p is the fluid pressure;

g is the gravitational acceleration;

$C_{\max}$ is the concentration that corresponds to the maximum density $\rho_{\max}$;

ρ_0 is the reference (freshwater) density;

ε is the density difference ratio defined as

$$\varepsilon = \frac{\rho_{\max}}{\rho_0} - 1 \tag{4}$$

where ρ is the density of the mixed fluid (fresh water and seawater).

The relationship between fluid density and concentration under isothermal conditions can be expressed in the form

$$\rho = \rho_0 \left(1 + \gamma C\right) = \rho_0 \left(1 + \rho_r\right) \tag{5}$$

where ρ_r is the relative density.

To describe solute transport, the following form of the modified Fokker-Planck equation is used:

$$\phi \frac{\partial C}{\partial t} = \nabla \cdot \left(\mathbf{D} \nabla C\right) - \nabla \cdot \left(C\mathbf{v}\right) \tag{6}$$

where

ϕ is the porosity and

$\mathbf{D} = \phi \overline{\mathbf{D}}$, with $\overline{\mathbf{D}}$ being the dispersion tensor that is time- and scale-dependent. A two-dimensional $x - z$ coordinate system for the tensor is given by

$$\begin{aligned} D_{xx} &= \left(\alpha_L \frac{v_x^2}{|\mathbf{v}|} + \alpha_T \frac{v_z^2}{|\mathbf{v}|} + D_d T_{xx} \right) t^{-\lambda}, D_{zz} = \left(\alpha_T \frac{v_x^2}{|\mathbf{v}|} + \alpha_L \frac{v_z^2}{|\mathbf{v}|} + D_d T_{zz} \right) t^{-\lambda}, \\ D_{xz} &= D_{zx} = \left(\left(\alpha_L - \alpha_T\right) \frac{v_x v_z}{|\mathbf{v}|} \right) t^{-\lambda} \end{aligned} \tag{7}$$

where

D_d is the molecular diffusion coefficient,

T_{xx} and T_{zz} are the principal components of the tortuosity tensor;

α_L and α_T are the longitudinal and transverse dispersivities respectively, and are defined as:

$$\alpha_L = \frac{D_{0x}}{2} \sigma^2 x^m, \alpha_T = \frac{D_{0z}}{2} \sigma^2 z^m \tag{8}$$

where

D_{0x} and D_{0z} are constants that are dependent on media properties;

σ^2 is the variance of the lower fractal cutoff limit subject to a fractal dimension d $(1.0 < d < 2.0)$;

λ is the exponent, $(0 < \lambda < 1.0)$, $m = 2d - 1$.

Equation (8) implies, as Wheatcraft and Tyler [1988] explained, that in a heterogeneous porous media there are two sources of variation in the flow travel path, namely, the fractal dimension that is a parameter measured over several scales, and fractal cutoff limit that causes variation on the microscopic scale.

Incorporating these two sources of variation in the classic Fokker-Planck equation improves the model's physical representation of transport processes which will be demonstrated by several the examples in Section 5..

It is interesting to note that for a mean value of λ and m, i.e., $\lambda = 1/2$ and $m = 3/2$, the fractal dispersivity has been shown by Wheatcraft and Tyler [1988, Eq. (16), p. 571-572] to give the best fit of the field data from extensive tracer studies carried out under different conditions [Gelhar, et al., 1985]. When $\lambda = 0$, α_L and α_T are constants i.e., $m = 0$ and (7) reduces to the same form given in Bear [1979].

The Darcy velocity vector may be expressed as

$$\mathbf{v} = -\mathbf{K}\left(\nabla h + \gamma C \nabla z\right) \tag{9}$$

To obtain a unique solution to (1) and (6), appropriate initial and boundary conditions must be specified.

For the flow equation, the initial condition may be expressed as

$$h(x, z; 0) = h_0(x, z) \text{ in } R \tag{10}$$

where

R is region of interest;

h_0 is the initial head.

The boundary conditions may be stated as follows:

Dirichlet boundary condition,

$$h(x_b, z_b; t) = h_d(x_b, z_b; t) \text{ in } B_d \tag{11}$$

Neumann boundary condition,

$$\mathbf{v} \cdot \mathbf{n} = V_n(x_b, z_b; t) \text{ in } B_n \tag{12}$$

where

$\mathbf{n}$ is the outward unit vector normal to the boundary;

(x_b, z_b) is a spatial coordinate on the boundary;

h_d and V_n are the Dirichlet functional value and Neumann flux, respectively.

For the transport equation, the initial condition may be expressed as

$$C(x, z; 0) = C_0(x, z) \quad \text{in } R \tag{13}$$

The boundary conditions may be stated as follows.

Dirichlet boundary condition:

$$C(x_b, z_b; t) = C_d(x_b, z_b; t) \text{ in } B_d \tag{14}$$

Neumann boundary condition:

$$n \cdot (-\mathbf{D}\nabla C) = V_n(x_b, z_b; t) \text{ in } B_n \tag{15}$$

Cauchy boundary conditions:

$$\mathbf{n} \cdot (C\mathbf{v} - \mathbf{D}\nabla C) = V_c(x_b, z_b; t) \text{ in } B_c \tag{16}$$

where C_d, V_n and V_c are the Dirichlet functional value , Neumann flux and Cauchy flux, respectively.

The exact boundary conditions used for each test problem will be explained in the results section of this paper.

3. Finite Volume Unstructured Mesh Methods

Over the past twenty years there has been great interest in the application of the Finite Volume (FV) or Control Volume (CV) approaches for solving fluid flow and heat transfer problems arising from computational fluid dynamics. Finite volume methods stem from an integral balance equation over a control volume. The success of these methods is due mainly to the conservative nature of the scheme and the fact that the terms appearing in the resulting algebraic equations have a specific physical implication.

In general, the FVUMMs can be categorised into two types, namely, vertex-centred and cell-centred. The classification of the approaches is based on the relationship between the control volume and the finite element like unstructured mesh [Chow, 1993].

The approach described here is the vertex-centred method generally known as the control volume based finite element mesh method by Baliga and Patankar [1988]. Ferguson and Turner [1996] and Perré and Turner [1999] have successfully used the method for studying the drying of wood. In a discrete solution, the solution domain is subdivided into smaller regions, nodes are distributed throughout the domain, and the connections between the nodes and the subregions form a mesh. In a finite element mesh, the subregions are called elements with the vertices of the elements being the nodal locations. For the vertex-centred approach only the basic elements are considered. To illustrate the control-volume definition and local-global co-ordinate transformation, only quadrilateral elements will be studied in this paper. A similar procedure has been developed elsewhere for triangular elements [Liu, et al, 2001].

In the solution domain, each node is associated with one control volume. Each surface of the control volume is defined as the vector that joins the centroid of the element to the midpoint of one of its sides as shown in Figure 1(a). Consequently, each of the elements is divided into several quadrants (four for a quadrilateral and three for a triangle) by these control surfaces (CS). These quadrilateral shapes are called sub-control

volumes (SCV) and illustrated in Figure 1(b). Thus, a control volume consists of the sum of all neighbouring SCVs that surround any given node. The CV is polygonal in shape and can be assembled in a straightforward and efficient manner at the element level. The flow and solute transport across each control surface must be determined by an integral. The FVUMM discretisation process is initiated by utilising the integrated form of Eqs. (1) and (6). Integrating the flow Eq. (1) and the transport Eq. (6) over an arbitrary control volume yields

$$\int_v S_s \frac{\partial h}{\partial t}\, dv = \int_v \nabla \cdot \left[\mathbf{K} \left(\nabla h + \gamma C \nabla z \right) \right] dv \tag{17}$$

$$\int_v \phi \frac{\partial C}{\partial t} dv = \int_V \nabla \cdot \left[\mathbf{D} \nabla C \right] dv - \int_V \nabla \cdot \left(C \mathbf{v} \right)\, dv \tag{18}$$

Applying the Gauss divergence theorem to the right-hand side of Eqs. (17) and (18) and using a lumped mass approach for the time derivative term gives

$$S_p \frac{\partial h_p}{\partial t} v_p = \int_S \left[\mathbf{K} \left(\nabla h + \gamma C \nabla z \right) \right] \cdot d\mathbf{n} \tag{19}$$

$$\phi \frac{\partial C_p}{\partial t} v_p = \int_S \left[\mathbf{D} \nabla C \right] \cdot d\mathbf{n} - \int_S \left(C \mathbf{v} \right) \cdot d\mathbf{n} \tag{20}$$

where

$d\mathbf{n}$ represents the components of the outward surface vector normal to the control surface S, and an anticlockwise traversal of the finite volume integration is assumed, i.e., $d\mathbf{n}$ can be approximated in the discrete sense by $d\mathbf{n} = \Delta z \hat{k} - \Delta x \hat{i}$; Δx and Δz represent the x and z components of the SCV face;

v_p is the area of the control volume, and is evaluated for the vertex case as

$$v_p = \sum_{i=1}^{N_{PSCV}} v_{SCV_i} \tag{21}$$

where

N_{PSCV} is the total number of SCV's that make up the control volume associated with the node p.

The integrals in Eqs. (19) and (20) are line integrals, which will be represented by the midpoint approximation for each control surface in order to attain second order accuracy. To approximate this midpoint, the argument of the integrals is required at the midpoint of the control surface and it is for these surfaces that the outward normal vector will be required.

The integral in Eq. (19) can be rewritten as

$$\int_S \left[\mathbf{K}\left(\nabla h + \gamma C \nabla z\right)\right]\cdot d\mathbf{n} = \sum_{j=1}^{N_{PSCV}} \int_{S_{j1}+S_{j2}} \left[\mathbf{K}^j\left(\nabla h^j + \gamma C^j \nabla z\right)\right]\cdot d\mathbf{n}^j$$

$$= \sum_{j=1}^{N_{PSCV}} \left\{ \sum_{r=1}^{2} \left[\left(K_{x,r}^j \frac{\partial h^j}{\partial x}\Delta z_r^j - K_{z,r}^j \frac{\partial h^j}{\partial z}\Delta x_r^j \right) - K_{z,r}^j \gamma C_r^j \Delta x_r^j \right] \right\} \tag{22}$$

The first integral on the right hand side of Eq. (20) can be rewritten as

$$\int_S \left[\mathbf{D}\nabla C\right]\cdot d\mathbf{n} = \sum_{j=1}^{N_{PSCV}} \int_{S_{j1}+S_{j2}} \left[\mathbf{D}^j \nabla C^j\right]\cdot d\mathbf{n}$$

$$= \sum_{j=1}^{N_{PSCV}} \left\{ \sum_{r=1}^{2} \left[\left(D_{xx,r}^j \frac{\partial C^j}{\partial x} + D_{xz,r}^j \frac{\partial C^j}{\partial z} \right)\Delta z_r^j - \left(D_{zx,r}^j \frac{\partial C^j}{\partial x} + D_{zz,r}^j \frac{\partial C^j}{\partial z} \right)\Delta x_r^j \right] \right\} \tag{23}$$

where

$$\begin{aligned} D_{xx,r}^j &= \left(\alpha_{L,r}^j \frac{v_{x,r}^2}{|\mathbf{v}_r|} + \alpha_{T,r}^j \frac{v_{z,r}^2}{|\mathbf{v}_r|} + D_d T_{xx} \right) t^{-\lambda}, \\ D_{zz,r}^j &= \left(\alpha_{T,r}^j \frac{v_{x,r}^2}{|\mathbf{v}_r|} + \alpha_{L,r}^j \frac{v_{z,r}^2}{|\mathbf{v}_r|} + D_d T_{zz} \right) t^{-\lambda}, \\ D_{xz,r}^j &= D_{zx,r}^j = \left(\left(\alpha_{L,r}^j - \alpha_{T,r}^j\right) \frac{v_{x,r} v_{z,r}}{|\mathbf{v}_r|} \right) t^{-\alpha} \end{aligned} \tag{24}$$

and

$$\alpha_{L,r}^j = \frac{D_{0x}}{2}\sigma^2\left(x_{IPr}^j\right)^m, \alpha_{T,r}^j = \frac{D_{0z}}{2}\sigma^2\left(z_{IPr}^j\right)^m \tag{25}$$

The second integral on the right hand side of Eq. (20) can be rewritten as

$$\int_S C\mathbf{v}\cdot d\mathbf{n} = -\int_S \left[C\mathbf{K}\left(\nabla h + \gamma C\nabla z\right)\right]\cdot d\mathbf{n}$$

$$= -\sum_{j=1}^{N_{PSCV}} \int_{S_{j1}+S_{j2}} C^j\left[\mathbf{K}^j\left(\nabla h^j + \gamma C^j \nabla z^j\right)\right]\cdot d\mathbf{n}$$

$$= -\sum_{j=1}^{N_{PSCV}} \left\{\sum_{r=1}^{2} C^j_{r,ups}\left[\left(K_x^j \frac{\partial h^j}{\partial x}\Delta z_r^j - K_z^j \frac{\partial h^j}{\partial z}\Delta x_r^j\right) - K_z^j \gamma C^j_{r,S}\Delta x_r^j\right]\right\} \tag{26}$$

where the upstream weighting technique will be used in this work (see Figure 2(b)):

$$C^j_{r,ups} = C^j_p, \text{ if } h^j_p \geq h^j_{p,r}\ ,\ C^j_{r,ups} = C^j_{x,r}, \text{ if } h^j_p < h^j_{p,r} \tag{27}$$

Upstream weighting can be shown to converge to the physically correct solution [Sammon, 1988] and has been used previously for saturated-unsaturated flow with dry initial conditions in heterogeneous media [Forsyth, et al, 1995].

To evaluate the terms in Eqs. (22), (23) and (26), a local-global co-ordinate transformation is introduced. It is convenient to work in a local co-ordinate system so that each element may be treated identically, irrespective of how distorted an element may be in terms of the global co-ordinates. Since the conservation law is applied in terms of global co-ordinates, it is necessary to relate the local and global co-ordinates. This is carried out as follows.

Let $\widehat{E} = [-1,1]\times[-1,1]$ be the reference square having the vertices $\widehat{A}_i\,(i = 1,2,3,4)$ (see Figure 1(c)). For every element E in the mesh, there exists a unique mapping: $\widehat{E} \to E$, given by

$$x = \sum_{i=1}^{4} x_i N_i(\xi,\eta), \quad z = \sum_{i=1}^{4} z_i N_i(\xi,\eta) \tag{28}$$

where $N_i(\xi,\eta)(i = 1,2,3,4)$ are bilinear shape functions on $\widehat{E}$, i.e.,

$$
\begin{aligned}
N_1(\xi,\eta) &= (1-\xi)(1-\eta)/4,\\
N_2(\xi,\eta) &= (1+\xi)(1-\eta)/4,\\
N_3(\xi,\eta) &= (1+\xi)(1+\eta)/4,\\
N_4(\xi,\eta) &= (1-\xi)(1+\eta)/4
\end{aligned}
\tag{29}
$$

and x_i, z_i are given global co-ordinates at local node i.

Using the chain rule for partial derivatives, the x and z derivatives of the shape functions can be determined, which, in matrix form, is written

$$
\begin{bmatrix} \frac{\partial N_i}{\partial \xi} \\ \frac{\partial N_i}{\partial \eta} \end{bmatrix} = \begin{bmatrix} \frac{\partial x}{\partial \xi} & \frac{\partial z}{\partial \xi} \\ \frac{\partial x}{\partial \eta} & \frac{\partial z}{\partial \eta} \end{bmatrix} \begin{bmatrix} \frac{\partial N_i}{\partial x} \\ \frac{\partial N_i}{\partial z} \end{bmatrix}
\tag{30}
$$

where

$$
\begin{aligned}
\frac{\partial x}{\partial \xi} &= \sum_{i=1}^{4} \frac{\partial N_i}{\partial \xi} x_i, \frac{\partial x}{\partial \eta} = \sum_{i=1}^{4} \frac{\partial N_i}{\partial \eta} x_i,\\
\frac{\partial z}{\partial \xi} &= \sum_{i=1}^{4} \frac{\partial N_i}{\partial \xi} z_i, \frac{\partial z}{\partial \eta} = \sum_{i=1}^{4} \frac{\partial N_i}{\partial \eta} z_i.
\end{aligned}
\tag{31}
$$

The local derivatives of the shape functions are determined by differentiating Eqs. (29):

$$
\begin{aligned}
\frac{\partial N_1}{\partial \xi} &= \frac{-(1-\eta)}{4}, \frac{\partial N_1}{\partial \eta} = \frac{-(1-\xi)}{4},\\
\frac{\partial N_2}{\partial \xi} &= \frac{(1-\eta)}{4}, \frac{\partial N_2}{\partial \eta} = \frac{-(1+\xi)}{4},\\
\frac{\partial N_3}{\partial \xi} &= \frac{(1+\eta)}{4}, \frac{\partial N_3}{\partial \eta} = \frac{(1+\xi)}{4},\\
\frac{\partial N_4}{\partial \xi} &= \frac{-(1+\eta)}{4}, \frac{\partial N_1}{\partial \eta} = \frac{(1-\xi)}{4}.
\end{aligned}
\tag{32}
$$

By solving the system (30) the derivatives of the N_i can be determined:

$$
\begin{bmatrix} \frac{\partial N_i}{\partial x} \\ \frac{\partial N_i}{\partial z} \end{bmatrix} = \frac{1}{J} \begin{bmatrix} \frac{\partial z}{\partial \eta} & \frac{-\partial z}{\partial \xi} \\ \frac{\partial x}{\partial \eta} & \frac{\partial x}{\partial \xi} \end{bmatrix} \begin{bmatrix} \frac{\partial N_i}{\partial \xi} \\ \frac{\partial N_i}{\partial \eta} \end{bmatrix} = \frac{1}{J} \begin{bmatrix} \frac{\partial z}{\partial \eta}\frac{\partial N_i}{\partial \xi} - \frac{\partial z}{\partial \xi}\frac{\partial N_i}{\partial \eta} \\ \frac{-\partial x}{\partial \eta}\frac{\partial N_i}{\partial \xi} + \frac{\partial x}{\partial \xi}\frac{\partial N_i}{\partial \eta} \end{bmatrix}
\tag{33}
$$

where

$$J = \frac{\partial x}{\partial \xi}\frac{\partial z}{\partial \eta} - \frac{\partial z}{\partial \xi}\frac{\partial x}{\partial \eta} \tag{34}$$

is the Jacobian of the transformation.

Any variable in the element may be defined if the nodal values are known. Let

$$h = \sum_{i=1}^{4} h_i N_i \tag{35}$$

$$C = \sum_{i=1}^{4} C_i N_i \tag{36}$$

The derivatives of any variable with respect to x and z within the element can be approximated in the same manner as the variable itself:

$$\begin{aligned} &\frac{\partial h}{\partial x} = \sum_{i=1}^{4} \frac{\partial N_i}{\partial x} h_i, \frac{\partial h}{\partial z} = \sum_{i=1}^{4} \frac{\partial N_i}{\partial z} h_i, \\ &\frac{\partial C}{\partial x} = \sum_{i=1}^{4} \frac{\partial N_i}{\partial x} C_i, \frac{\partial C}{\partial z} = \sum_{i=1}^{4} \frac{\partial N_i}{\partial z} C_i. \end{aligned} \tag{37}$$

If the approximations to the global derivatives are used, Eqs. (35), (36) and (37) are substituted into Eqs. (22), (23), (26), and the final form of the discretised equations becomes

$$\begin{aligned} &S_s \frac{\partial h_p}{\partial t} v_p \\ &= \sum_{j=1}^{N_{PSCV}} \left\{ \sum_{r=1}^{2} \left[\sum_{l=1}^{N_{vert}} \left(K_x^j \frac{\partial N_l^j}{\partial x} \Delta z_{lr}^j - K_y^j \frac{\partial N_l^j}{\partial z} \Delta x_{lr}^j \right) h_l^j - K_y^j \gamma C_{r,S}^j \Delta x_{lr}^j \right] \right\} \end{aligned} \tag{38}$$

$$\begin{aligned} &\phi \frac{\partial C_p}{\partial t} v_p \\ &= \sum_{j=1}^{N_{PSCV}} \left\{ \sum_{r=1}^{2} \sum_{l=1}^{N_{vert}} \left[\left(D_{xx,r}^j \frac{\partial N_l^j}{\partial x} + D_{xz,r}^j \frac{\partial N_l^j}{\partial z} \right) \Delta z_{lr}^j - \left(D_{zx,r}^j \frac{\partial N_l^j}{\partial x} + D_{zz,r}^j \frac{\partial N_l^j}{\partial z} \right) \Delta x_{lr}^j \right] C_l^j \right\} \\ &+ \sum_{j=1}^{N_{PSCV}} \left\{ \sum_{r=1}^{2} C_{r,ups}^j \left[\sum_{l=1}^{N_{vert}} \left(K_x^j \frac{\partial N_i^j}{\partial x} \Delta z_{lr}^j - K_z^j \frac{\partial N_i^j}{\partial z} \Delta x_{lr}^j \right) h_l^j - K_z^j \gamma C_{r,S}^j \Delta x_{lr}^j \right] \right\} \end{aligned} \tag{39}$$

where N_{vert} represent the number of vertices of the finite element.

The concentration $C_{r,S}^{j}$ in the gravitational term within each SCV is represented by the use of shape functions at the midpoint ($IPr(x_{IPr}, z_{IPr}), r = 1,2$) of each SCV, i.e., the $C_{r,S}^{j}$ will be evaluated at the SCV integration point for each face (see Figure 2):

$$C_{r,S}^{j} = \sum_{i=1}^{4} C_i^j N_i \left(x_{IPr}, z_{IPr} \right) \tag{40}$$

The components of the fluid velocity will be approximated by

$$\begin{aligned} &\left| \mathbf{v}_r \right| = \sqrt{v_{x,r}^2 + v_{z,r}^2}, v_{x,r} = -\sum_{l=1}^{N_{vert}} K_x^j \frac{\partial N_i^j}{\partial x} \Delta z_{lr}^j h_l^j, \\ &v_{z,r} = \sum_{l=1}^{N_{vert}} K_z^j \frac{\partial N_i^j}{\partial z} \Delta x_{lr}^j h_l^j + K_z^j \eta C_{r,S}^j \Delta x_{lr}^j. \end{aligned} \tag{41}$$

4. Numerical Treatment of the Problem

Equations (1) and (6) are transformed into a system of ordinary differential equations (ODE) of the form (38) and (39) for each node using FVUMM as described in the above section. The two ODEs represented by (38) and (39) are linked by the terms containing the density-coupling coefficient γ via the Darcy's velocities. The density-coupling terms make the transport problem nonlinear. For the case in which the buoyancy effects dominate, convergence difficulties are often encountered when performing steady state simulations. A large number of numerical techniques have been developed for the time-discretization of this system. In particular, Frind [1982b] used a time-weighted form, Huyakorn et al. [1987] used an implicit Picard iterative scheme with sequential solution procedure that incorporates salient features designed to enhance convergence of the non-linear iterative solution. These features include (i) the use of time-extrapolation formulas for obtaining an initial estimate of the nodal values of head and concentration at the end of a current time step; (ii) the use of an automatic underrelaxation scheme for predicting

the head and concentration values for the next iteration; and (iii) automatic reduction of time step values when the prescribed number of nonlinear iterations is exceeded.

In this paper, the complete ODE system is solved numerically using the differential algebraic system solver package DASSL. This program uses the backward differentiation formulas of orders one to five to solve a system of differential-algebraic equations (Petzold, 1982). The code automatically selects an initial step size that is practically always suitable for the problem. Time step sizes are adapted during processing to achieve the desired accuracy. To solve differential/algebraic problems it is necessary to resolve a non-linear system of equations using Newton's method. In this code, the Jacobian matrix is approximated numerically. The time integration order is selected automatically depending on the condition of the system. This numerical technique has been used to solve adsorption problems involving steep gradients in bidisperse particles (Liu and Bhatia, 1999), hyperbolic models of transport in bidisperse solids (Liu and Bhatia, 2000) and numerical models of adsorption problems [Bhatia, et al, 2000; Liu and Bhatia, 2001a, 2001b). In this discretisation, a lumped mass and upstream weighting techniques are used.

In order to close the system, the boundary conditions must be also numerically treated. After the assembly of the nodal control volume equations, complete conservation equations will result for all interior control volumes. However, at solution boundaries, the corresponding control volume has two control surfaces to which boundary conditions must be applied in order to complete the equations of conservation. Figure 4 illustrates sub-control volumes for a quadrilateral element where two of its sides form part of the solution domain boundary. In evaluating the boundary conditions along these sides, boundary integration points (BIP) and the corresponding boundary control surfaces (BCS) are needed, as shown in Figure (d). The usual boundary conditions (27), (28), (29), (30), (31) and (32) can now be easily and directly applied.

5. Numerical Simulation Results

In the following, we examine the following situations:

[1] the case where $\alpha_L = 0, \alpha_T = 0$ and $D_d \neq 0$ will be referred to as a constant coefficient dispersion;

[2] the case where $\alpha_L \neq 0,\ \alpha_T \neq 0,\ D_d = 0$ will be referred to as variable coefficient dispersion;

[3] If $\lambda > 0,\ m \neq 0,$ this case will be referred to as time- and scale- dependent dispersion.

Example 1: Seawater Intrusion in a Confined Aquifer

This example is concerned with groundwater flow and salt transport in a confined coastal aquifer, which is known widely as Henry's saltwater intrusion problem [Henry, 1959], and described schematically in Figure 2. The transient analyses were performed. The parameters were chosen so that the cases analyzed correspond to those solved numerically by others [Huyakorn et al., 1987; Cheng et al., 1998]. The boundary conditions employed in our numerical simulation are also shown. The aquifer under consideration is a uniform isotropic aquifer that is bounded below and above by impermeable strata. In addition, the aquifer is exposed on the right side to a stationary saltwater body and is recharged on the left side by a constant freshwater influx. The coastal boundary condition allows convective mass transport out of the system over the top portion $(80m \le z \le 100m)$. Therefore, the normal concentration gradient is set to zero. The initial concentration and reference hydraulic head were also set to zero.

The aquifer region was represented by a two-dimensional regular rectangular mesh consisting of 150 (15×10) elements and 176 (16×11) nodes.

Case 1. Variable dispersion: D_d was set to zero, and the longitudinal and transverse dispersivities α_L and α_T were set to 3.5 m, $\lambda = 0$ and $m = 0$.

Figure 3(a) shows the 0.5-isochlor distributions using FVUMM for the transient state at t=4000 days. It is apparent from Figure 3(a) that the present analysis is in good agreement with those of Cheng et al. [1998], Huyakorn et al. [1987] and Frind [1982b], instilling confidence in the numerical methods used to solve the problem.

Case 2. Time- and scale-dependent dispersion : D_d was set to zero, λ was set to ½, and the longitudinal and transverse dispersivities α_L and α_T were set to $3.5x^{3/2}$ m and $3.5z^{3/2}$ m, i.e., $\alpha_L = \frac{D_{0x}}{2}\sigma^2 = 3.5$, $\alpha_T = \frac{D_{0z}}{2}\sigma^2 = 3.5$, $m = \frac{2}{3}$, in order to investigate and compare with Henry's saltwater intrusion problem.

Figure 3(b) shows the isochlor distributions using FVUMM for the transient state at t=4000 days. From Figure 3(b) , it can be seen that the salt front moves from the right side to the left side across the aquifer. Furthermore, as a result of the enhanced dispersion, and also the increased convective mixing in the upper layer, salts move faster in the upper layer. This type of profile reflects a more realistic shape of a transition zone between a a seawater/freshwater interface observed in the field [Konikow and Reilley, 2000, Fig.13.5, p. 472; Voss, 2000, Fig. 9.6, p. 283].

Case 3. Constant dispersion: the molecular diffusion coefficient D_d was set to $6.6\times10^{-2} m^2/d$, α_L and α_T were set to zero, $\lambda = 0$ and $m = 0$.

Figure 3(c) shows the reference head and the 0.5-isochlor distributions using FVUMM for the transient state simulation at t=4000 days. From Figure 3(c), it is seen that the result is in satisfactory agreement with published solutions [Frind, 1982b; Huyakorn et al., 1987; Cheng et al., 1998].

Example 2: Seawater Intrusion in Phreatic Aquifer

The methods described in this paper can also be applied to simulate the steady-state problem. In order to justify this, a steady-state problem of seawater intrusion in

phreatic was investigated. The problem considered in this example is described schematically in Figure 4(a) and involves an anisotropic unconfined aquifer. The aquifer is recharged by freshwater from the top and from the landward side, and invaded by saltwater on the coastal side [Cheng, et al., 1998 and Huyakorn et al., 1987]. The saturated thickness is assumed to be 50m. In addition, the top boundary of the phreatic aquifer, which is a free surface, is assumed to be fixed at an elevation of 50m above the base of the aquifer. The region of interest was discretized into 250 (10×25) rectangular elements and 286 nodes.

Figure 4(b) shows the 0.5-isochlor distributions using FVUMM for the transient state at t=2000 days, the relative least squares errors are 10^{-10} for the reference head and 10^{-7} for the concentration, respectively. This transient simulation was performed to compare the results of a steady-state simulation with those of Huyakorn et al. [1987], Galeati, et al, [1992] and Cheng et al. [1998]. The initial values of the reference hydraulic head and concentration were set to zero. It is apparent from Figure 4(b) that the present analysis is in good agreement with those of Cheng et al. [1998], Huyakorn et al. [1987] and Galeati et al. [1992].

Example 3: Leachate transport in unconfined aquifer

Sanitary landfill or industrial waste disposal sites often cause groundwater contamination when leachates reach the watertable. The problem considered in this example is described schematically in Figure 5 [see Frind, 1982b]. In the example, a disposal site is situated on the ground surface above the watertable, and unprotected from precipitation. Because the disposal site is not in direct contact with the watertable, mass input to the groundwater system is by way of the natural recharge, which is assumed to become chemically saturated with leachate in the wastes. This situation is represented by the Cauchy boundary condition, where unsaturated flow is neglected, recharge and mass

input are taken to be constant in time. The aquifer is unconfined, 24m thick, and 3000m in length. The region of interest was discretized into $760\left((3+40+52)\times 8\right)$ rectangular elements and 864 nodes.

The case of transient state simulations was used to show the evolution of the leachate plume in the aquifer. This transient simulation is based on an initial condition of no leachate in the aquifer. Figure 6 shows the leachate distribution in the aquifer at (a) 1.5 years, (b) 3 years, (c) 6 years and (d) 12 years. It can be seen from Figure 6 that the leachate at first advances more or less in a downward direction into the aquifer. The advance is due mainly to transverse dispersion and to the recharge flux, while density has little effect. Later, the concentration begins to build up under the downstream edge of the site as a result of convection from the site, which is found to be nearly uniform across the aquifer thickness at later times because of relatively large vertical dispersion in the system. The results depicted here exhibit similar treads to those reported by Frind [1982b].

6. Conclusion

In this paper, finite volume methods for the transient simulation of time-, scale- and density-dependent transport have been described and demonstrated. Comparisons are made to several conventional cases where the dispersivity is not a function of either time or scale. It is shown that with a time- and scale-dependent dispersivity in the MFPE the simulated saltwater concentration isochlors better capture experimental observation in comparison with previous published results.

Despite the detailed analysis of the model using the numerical method presented in the paper, it is clear that more detailed investigations are required to analyse the new mathematical model and compare the simulations with field data under different conditions. Further investigations will clarify the variability and sensitivity of the

parameters, and further clarify their implications. This paper does not intend to cover all of these aspects due to the scale and magnitude of the work involved.

The methods can be readily applied to the steady-state problem. The method and techniques discussed in this paper can also be extended to three-dimensional problems which will be the subject of future work.

Acknowledgements

This research has been supported by the ARC SPIRT grant C10024101.

References

Baliga, B. R. and S. V. Patanka, Elliptic system: finite element I**.** *Handbook of Numerical Heat Transfer*, Editors W. J. Minkowycz et al., Wiley, 1988.

Bear, J., *Hydraulics of Groundwater*, McGraw-Hill, New York, 1979.

Bhatia, S. K., F. Liu, and G. Arvind, Effect of Pore Blockage on Adsorption Isotherms and Dynamics: Anomalous Adsorption of Iodine in Activated Carbon, *Langmuir*, 16, 4001–4008, 2000.

Cheng, J. R., R. O. Strobl, G. T. Yeh, G.T., H. C. Lin, and W. H. Choi, Modeling of 2D density-dependent flow and transport in the subsurface," *J. Hydro*. *Eng*., 3(4), 248–257, 1998.

Chow, P. M., Control volume unstructured mesh procedure for convection-diffusion solidification processes, *Ph.D thesis*, University of Greenwich, London, 1993.

Dieulin, A., G. Matheron, G. de Marsily, and B. Beaudoin, Time dependence of an "equivalent dispersion coefficient" for transport in porous media, *Proc. Euromech*, 143, Delft. In: A. Veruijt and F. B. J. Barends (eds.), 199–202, Balkema, Rotterdam, 1981.

Frind, E. O., Seawater intrusion in continuous coastal aquifer-aquitard systems, *Adv. Water Resour*, 5(2), 89–97, 1982a.

Frind, E. O., Simulation of long-term trasient density-dependent transport in groudwater, *Adv. Water Resour*, 5(2), 73–88, 1982b.

Ferguson, W. J. and I. W. Turner, A control volume finite element numerical simulation of the Drying of Spruce, *J. Comp. Phys*., 125, 59–70, 1996.

Forsyth, P. A., Y. S. Wu, and K. Pruess, Robust numerical methods for saturated-unsaturated flow with dry initial conditions in heterogeneous media, *Adv. Water Resour*, 18, 25–38, 1995.

Gelhar, L. W., C. Welty, and K. R. Rehfeldt, A critical review of data on field-scale dispersion in aquifers, *Water Resour. Res.*, 28(7), 1955–1974, 1992.

Gelhar, L. W. A. Mantoglou, C. Welty, and K. L. Rehfeldt, 1985 A review of field scale physical solute transport processes in saturated and unsaturated porous media. *Rep. EA-4190*, Electro. Power Res. Ins., Palo Alto, Calif., 1985.

Henry, H. R., Salt intrusion into freshwater aquifers, *J. Geophyd. Res*., 64, 1911–1919, 1959.

Henry, H. R., Effects of dispersion on salt encroachment in coastal aquifers, in Sea Water in Coastal Aquifers, H. H. Cooper et al. (eds): *US Geological Survey Water Supply Paper* 1613-C, 1964.

Hentschel, H. G. E., and I. Procaccia, I. 1984 Relative diffusion in turbulent media: The fractal dimension of clouds, *Physical Review A*, 29(3), 1461–1470.

Huyakorn, P. S. P. F. Andersen, J. W. Mercer, and H. O. White Jr., Saltwater intrusion in aquifers: Develpoment and testing of a three-dimensional finite element model," *Water Resour. Res*., 23(2), 293–312, 1987.

Konikow, L. F., and T. E. Reilly, Seawater intrusion in the United States. Chapter 13 in: J. Bear et al. (eds.): Seawater Intrusion in Coastal Aquifers – Concepts, Methods and Practices, p. 463–506, Kluwer, Dordrecht. 2000.

Lallemand-Barrés, A., and P. Peaudecerf, Recherche des relations entre les valeurs mesurées de la dispersivité macroscopique d'un millieu aquifére, ses autres caractéristiques, et les conditions de mesure, *Bull. Bur. Rech. Geol. Min. Fr., Sect*. 3, 277–284, 1978.

Liu, F., and S. K. Bhatia, Computationally efficient solution techniques for adsorption problems involving steep gradients in bidisperse particles, *Comp. Chem*. *Eng*., 23, 933-943, 1999.

Liu, F., and S. K. Bhatia, Numerical solution of hyperbolic models of transport in bidisperse solids." *Comp. Chem*. *Eng*., 24, 1981–1995, 2000.

Liu, F., and S. K. Bhatia, S. K. Application of Petrov-Galerkin Methods to Transient Boundary Value Problems in Chemical Engineering: Adsorption with Steep Gradients in Bidisperse Solids, *Chem. Eng*. Sci., 56, 3727-3735, 2001.

Liu, F., and S. K. Bhatia, Solution Techniques for Transport Problems Involving Steep Concentration Gradients: Application to Noncatalytic Fluid-Solid Reactions, *Comp. Chem. Eng*., in press, 2001.

Liu, F., I. W. Turner, and V. Anh, A finite volume unstructured mesh method for Modelling saltwater intrusion into aquifer systems, *The proceedings of the First International Conference on Saltwater Intrusion and Coastal Aquifer: Monitoring, Modelling and Management*, Essaouira, Morocco, 2001.

Muralidhar, R. and D. Ramkrishna, Diffusion in pore fractals: A review of linear response model, *Transport in Porous Media*, 13, 79–95, 1993.

Neuman, S. P., Universal scaling of hydraulic conductivities and dispersivities in geologic media, *Water Resour. Res.*, 26(8), 1749–1758, 1990.

Pelzold, L. R., A description of DASSL: a differential/algebraic equation system solver, *Technical Report No. SAND 82-8637*, Sandia National Laboratories, Livermore, 1982.

Perré P., and I. W. Turner, TransPore: A Generic Heat and Mass Transfer Computational Model for Understanding and Visualising The Drying Of Porous Media, *Drying Technology Journal*, 17(7), 1273–1289, 1999.

Patankar, S. V., Numerical Heat Transfer and Fluid Flow, *McGraw-Hill*, New York, 1980.

Segol, G., G. F. Pinder, and W. G. Gray, A galerkin finite element technique for calculating the transient position of the saltwater front, *Water Resour Res*., 11(2), 343–347, 1975.

Sammon, P., An analysis of upstream weighting, *SPE J. RES. Eng*., 3, 1053–1056, 1988.

Voss, C. I., AQUIFEM-SALT: A Finite-element model for aquifers containing a seawater interface, *USGS Water Resour. Invest. Rpt*. 84–4263, 1984.

Voss, C. I., USGS SUTRA Code – History, Practical Use and Applications in Hawaii, Chapter 9 in: J. Bear et al (eds.) Seawater Intrusion in Coastal Aquifers – Concepts, Methods and Practices, Kluwer, Dordrecht. Bear et al (eds.) Seawater Intrusion in Coastal Aquifers – Concepts, Methods and Practices, p. 249–313, Kluwer, Dordrecht, 2000.

Wheateraft, S.W., and S. W. Tyler, 1988 An explanation of scale-dependent dispersivity in heterogeneous aquifers using concepts of fractal geometry, *Water Resour Res*., 24(4), 566–578, 1988.

LIST OF FIRURES

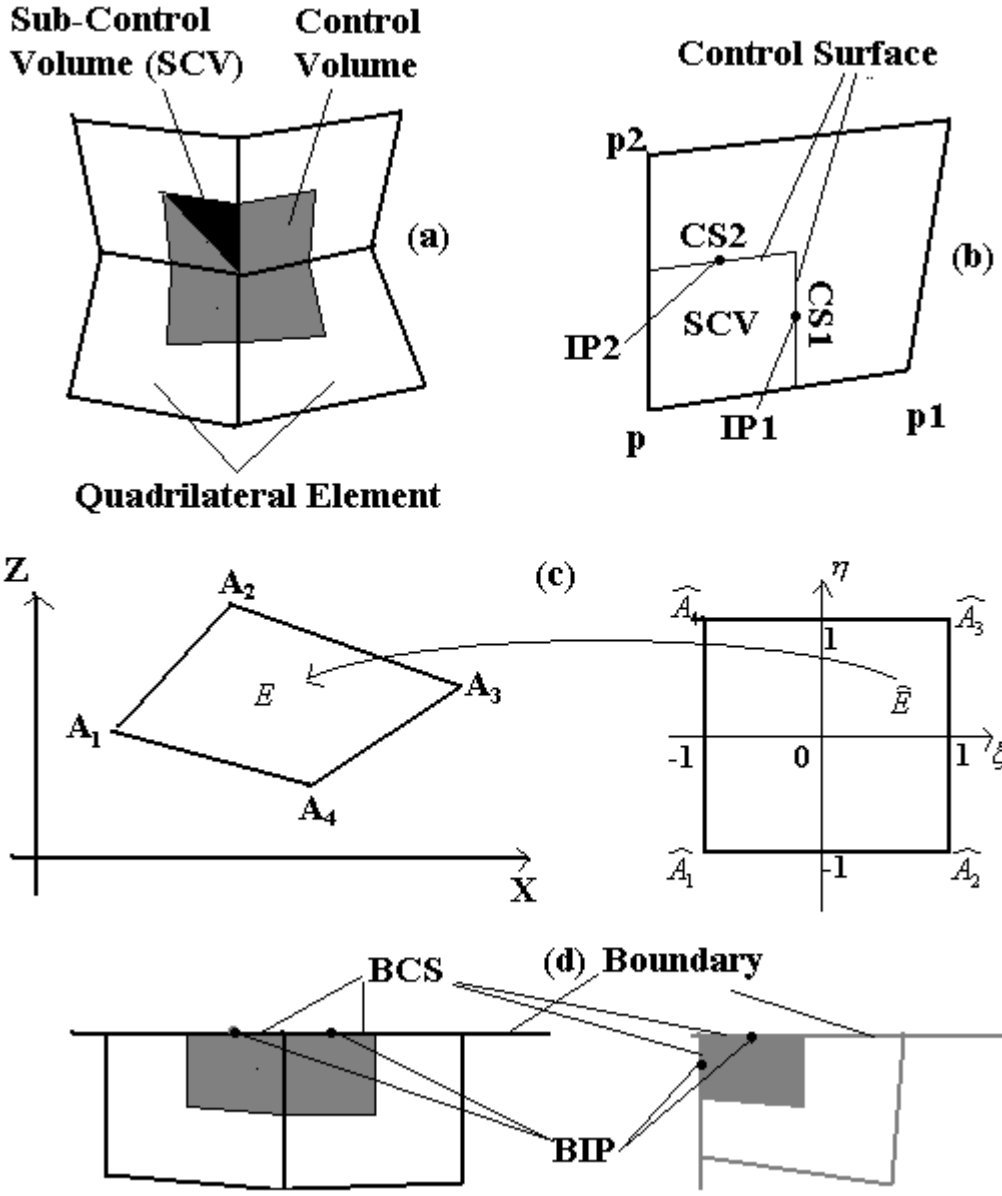
Sub-Control Volume (SCV)
Control Volume
(a)
Quadrilateral Element
Control Surface
p2
CS2
(b)
IP2
SCV
CS1
p
IP1
p1
Z
A2
(c)
E
A3
A1
A4
X
η
1
-1
0
1
ξ
-1
BCS
(d) Boundary
BIP

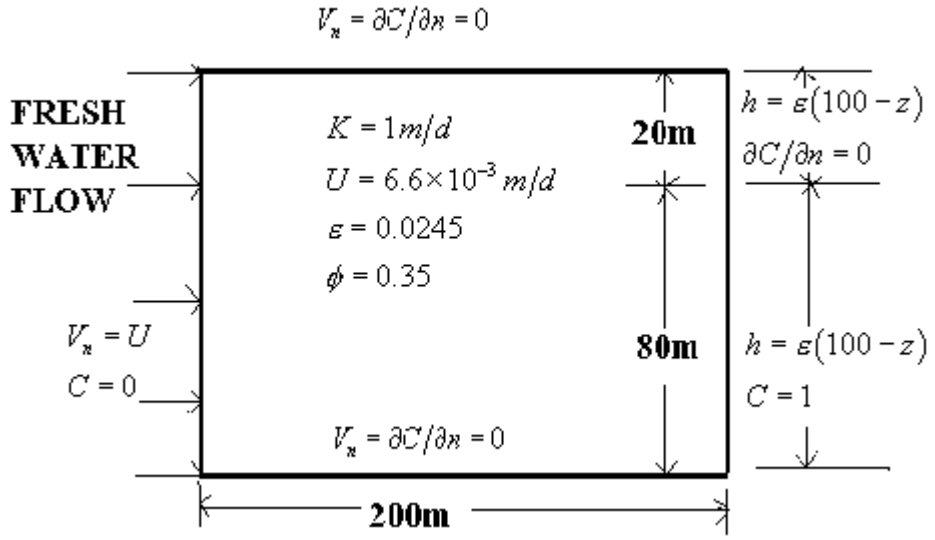
$V_n = \partial C/\partial n = 0$
FRESH
WATER
FLOW
$K = 1 m/d$
$U = 6.6\times10^{-3} m/d$
$\varepsilon = 0.0245$
$\phi = 0.35$
20m
80m
$h = \varepsilon(100 - z)$
$\partial C/\partial n = 0$
$h = \varepsilon(100 - z)$
$C = 1$
$V_n = U$
$C = 0$
$V_n = \partial C/\partial n = 0$
200m

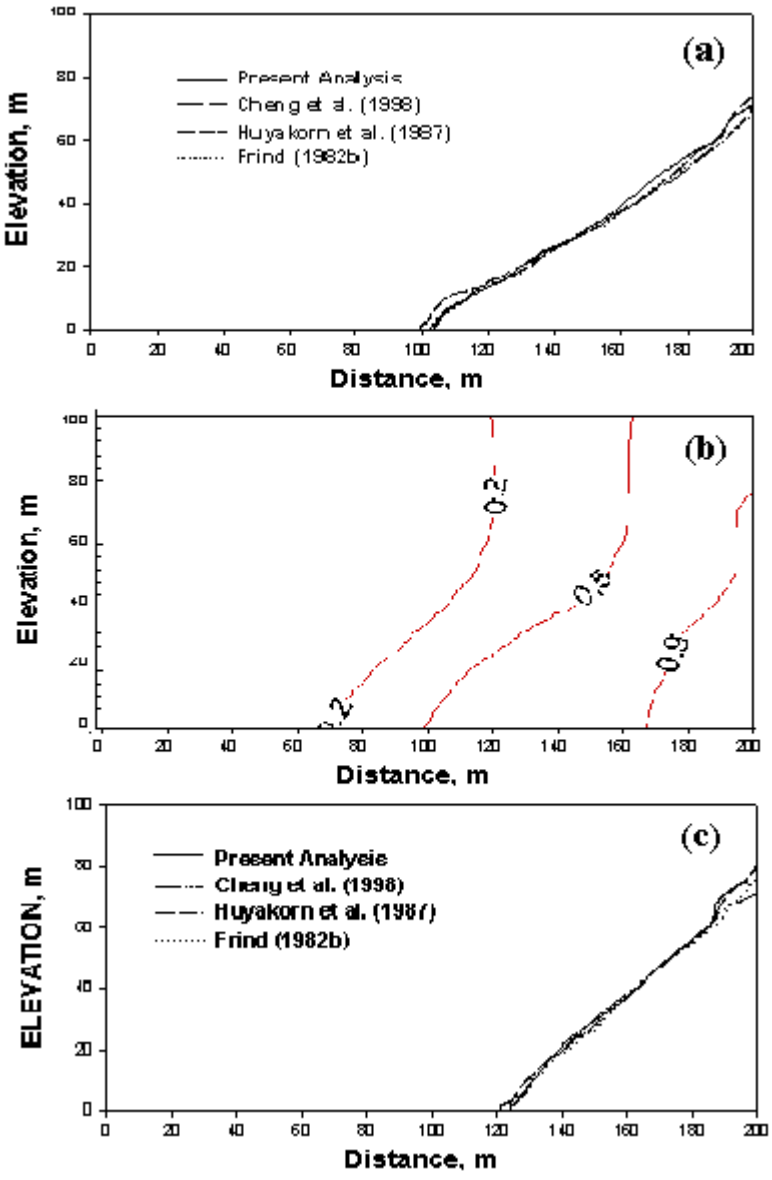
(a)
Present Analysis
Cheng et al. (1998)
Huyakorn et al. (1987)
Frind (1982b)
Elevation, m
Distance, m
(b)
0.2
0.5
0.9
Elevation, m
Distance, m
(c)
Present Analysis
Cheng et al. (1998)
Huyakorn et al. (1987)
Frind (1982b)
ELEVATION, m
Distance, m

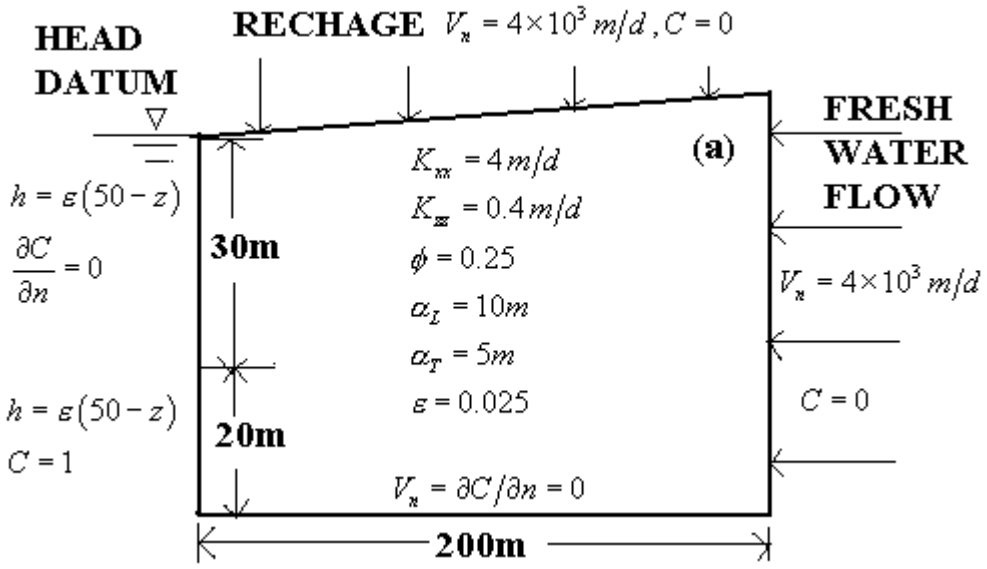
HEAD
DATUM
RECHAGE $V_n = 4\times10^3\ m/d\ , C = 0$
FRESH
WATER
FLOW
(a)
$K_{xx} = 4\ m/d$
$K_{zz} = 0.4\ m/d$
$\phi = 0.25$
$\alpha_L = 10m$
$\alpha_T = 5m$
$\varepsilon = 0.025$
$h = \varepsilon(50 - z)$
$\frac{\partial C}{\partial n} = 0$
30m
20m
$h = \varepsilon(50 - z)$
$C = 1$
$V_n = 4\times10^3\ m/d$
$C = 0$
$V_n = \partial C/\partial n = 0$
200m

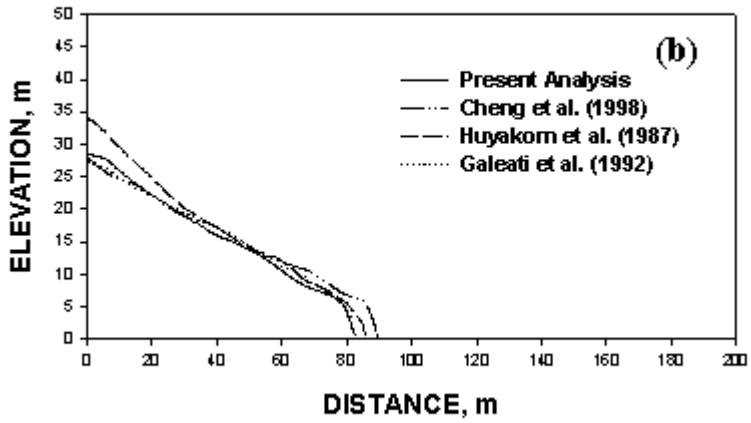
(b)
Present Analysis
Cheng et al. (1998)
Huyakorn et al. (1987)
Galeati et al. (1992)
ELEVATION, m
DISTANCE, m
0
5
10
15
20
25
30
35
40
45
50
0
20
40
60
80
100
120
140
160
180
200

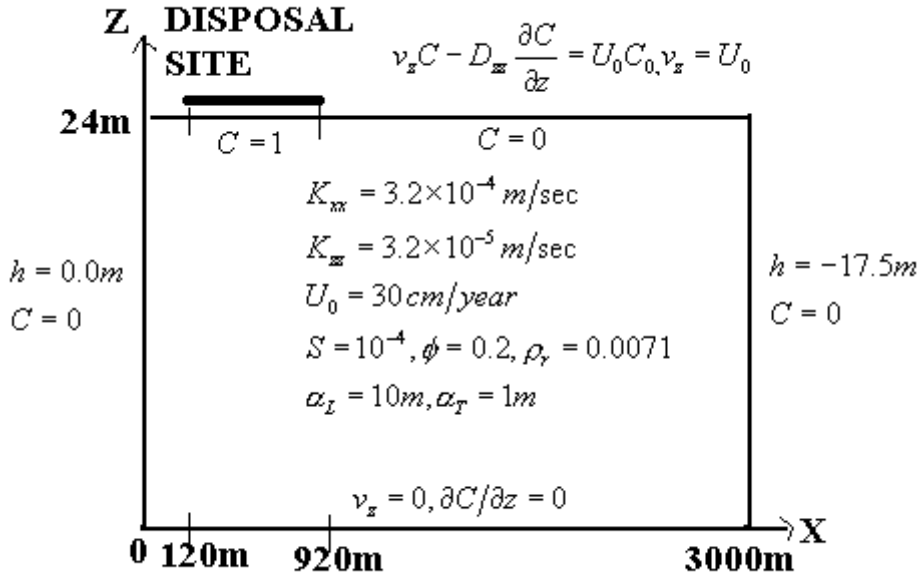
Z
DISPOSAL SITE
$v_z C - D_{zz}\frac{\partial C}{\partial z} = U_0 C_0, v_z = U_0$
24m
$C = 1$
$C = 0$
$K_{xx} = 3.2\times10^{-4}\ m/\sec$
$K_{zz} = 3.2\times10^{-5}\ m/\sec$
$U_0 = 30\,cm/year$
$S = 10^{-4}, \phi = 0.2, \rho_r = 0.0071$
$\alpha_L = 10m, \alpha_T = 1m$
$h = 0.0m$
$C = 0$
$h = -17.5m$
$C = 0$
$v_z = 0, \partial C/\partial z = 0$
X
0
120m
920m
3000m

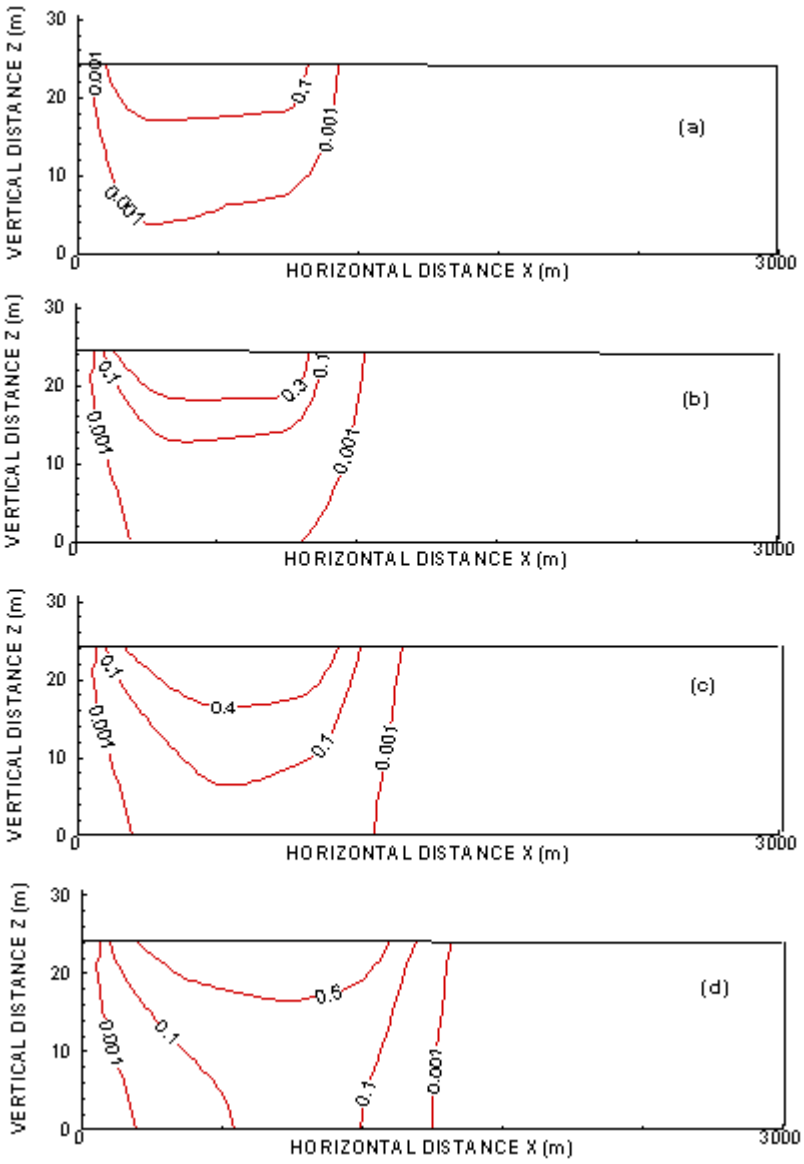
VERTICAL DISTANCE Z (m)
30
20
10
0
0.001
0.7
0.001
0.001
(a)
0
HORIZONTAL DISTANCE X (m)
3000
VERTICAL DISTANCE Z (m)
30
20
10
0
0.1
0.3
0.1
0.001
0.001
(b)
0
HORIZONTAL DISTANCE X (m)
3000
VERTICAL DISTANCE Z (m)
30
20
10
0
0.1
0.4
0.001
0.1
0.001
(c)
0
HORIZONTAL DISTANCE X (m)
3000
VERTICAL DISTANCE Z (m)
30
20
10
0
0.5
0.001
0.1
0.1
0.001
(d)
0
HORIZONTAL DISTANCE X (m)
3000